Available online at www.sciencedirect.com
ScienceDirect
Journal of Power Sources 172 (2007) 530–541
JOURNAL OF POWER SOURCES
www.elsevier.com/locate/jpowsour

# Evaluation of electrochemical performance for surface-modified carbons as catalyst support in polymer electrolyte membrane (PEM) fuel cells

Abhishek Guha [a], Thomas A. Zawodzinski Jr. [b], David A. Schiraldi [a,*]

[a] *Department of Macromolecular Science and Engineering and Case Advanced Power Institute, Case Western Reserve University, Cleveland, OH 44106, USA*
[b] *Department of Chemical Engineering, Case Advanced Power Institute, Case Western Reserve University, Cleveland, OH 44106, USA*

Received 10 May 2007; accepted 13 July 2007
Available online 25 July 2007

**Abstract**

The electrochemical performance of platinum (Pt) catalyst deposited on various functionalized carbon supports was investigated and compared with that of a commercial catalyst, Pt on Vulcan XC-72 carbon. The supports employed were graphitic or amorphous with a wide range of surface areas. Cyclic voltammetry (CV) and rotating disk electrode (RDE) studies on the supported catalysts indicated equivalent platinum catalyst activities. Fuel cell performance was determined for membrane electrode assemblies (MEA) fabricated from the supported catalysts. The use of high surface area supports did not necessarily translate into a higher electrochemical utilization of platinum. Electrochemical impedance spectroscopy (EIS) measurements indicated lower ohmic losses for low surface area carbon MEAs. This is explained by the supported catalyst electrode microstructures and their intrinsic resistivities. Correlation of all data indicates that for low surface carbons, nature of the support does not significantly affect the Pt catalytic activity. The influence of the support is more critical when high surface area carbons are used because of the vastly different electrode morphology and resistivity.
© 2007 Elsevier B.V. All rights reserved.

*Keywords:* Carbon nanofibers; Activated carbon; Catalyst support; Fuel cells; Electrochemical properties; Electrical conductivity

## 1. Introduction

Various forms of surface-modified carbons have been investigated as supports for precious metal catalysts [1–4]. Such carbons exhibit numerous advantages over rival supports making them the material of choice for supporting catalyst particles. In polymer electrolyte membrane (PEM) fuel cells, also known as proton exchange membrane fuel cells, carbons with varying catalyst loadings are commonly employed as composite electrodes. Homogeneous deposition of the catalyst on carbon support is generally believed to be critical to optimum catalytic activity. Such a deposition assists towards attainment of a 'three-phase boundary layer' in the membrane electrode assembly (MEA). A catalyst particle within such a boundary layer is intimately connected to the support and membrane by a layer of ionomer [5,6]. Such a contact ensures superior proton transport and aids in electron conduction through the external circuit. Numerous publications have emphasized the importance of chemically modifying the carbon support in order to make the carbon surface amenable for catalyst deposition [7–9]. Our recent work has demonstrated the potential for replacement of the currently popular carbon support, Vulcan® XC-72 carbon black, with attractive carbon varieties such as carbon nanofibers and activated carbon [10]. The viability of these supported catalysts employing non-traditional carbon supports is evaluated herein.

This study compares the electrochemical performance of platinum (Pt) catalyst supported on several nitric acid-modified carbon varieties, both graphitic and amorphous in nature. Prominent electrochemical parameters such as the electrochemically active surface areas (ESA) of platinum and the

* Corresponding author at: Department of Macromolecular Science and Engineering, Case Western Reserve University, 538 Kent Hale Smith Building, 2100 Adelbert Road, Cleveland 44106-7202, USA. Tel.: +1 216 368 4243; fax: +1 216 368 4202.
*E-mail address:* das44@cwru.edu (D.A. Schiraldi).

0378-7753/$ – see front matter © 2007 Elsevier B.V. All rights reserved.
doi:10.1016/j.jpowsour.2007.07.035

intrinsic activity for oxygen reduction reaction (ORR) have been determined. The values obtained for the various supported catalyst systems are compared with the commercially available Pt/Vulcan XC-72 catalyst. ESA of platinum catalyst on the carbon support in the 'as-prepared state' has been calculated by the hydrogen adsorption/desorption charge measured via cyclic voltammetry (CV) [11].ESA of platinum catalyst on the carbon support within the MEA has also been determined by carbon monoxide (CO) stripping voltammetry [12–15]. The relative intrinsic activity of the supported catalysts towards accelerating the oxygen reduction reaction occurring at the cathode of a PEM fuel cell is investigated by rotating disk electrode (RDE) measurements, as highlighted in a number of papers [16–18]. To justify practical applicability, performance of the supported catalyst is evaluated in a working fuel cell environment. We have attempted to quantify the overall ohmic resistance of the cell, a major contributor towards performance loss, by electrochemical impedance spectroscopy (EIS).

The microstructure of the supported catalyst layer together with electrochemical properties of the catalyst determines overall performance of the fuel cell electrode. Hence, an investigation into the support microstructure is critical and we have likewise attempted to correlate the trend in overall cell resistance with morphological characteristics of the supported catalyst electrodes. Such a trend, which influences the overall performance of the MEA (and hence the fuel cell), is also potentially dictated by the electronic conductivity of the supported catalyst. Therefore, electrical resistances of the various carbon supported catalyst systems have been measured and the calculated resistivity/conductivity values compared.

## 2. Experimental

### 2.1. Materials

Two types of carbon support were studied in this work. Graphitic carbon nanofibers or CNF (Pyrograf®-III; PR-19-HHT grade) were obtained from Applied Sciences Inc., Cedarville, OH; while amorphous activated carbons or AC (Norit® SX Ultra Cat, Norit® SX Plus Cat and Norit® DLC Supra 50) were supplied by Norit Americas Inc., Marshall, TX. The nanofibers exist as coaxial graphene cylinders with hollow cores. The SX Ultra Cat and SX Plus Cat grades consist of a combination of *meso*- and *micro*-pores and are manufactured specifically for catalyst support applications. The DLC Supra 50 grade is predominantly microporous. Table 1 highlights physical properties of the 'as-received' particulate activated carbon grades.

### 2.2. Functionalization of carbon [10]

Each carbon support sample was functionalized by treatment with nitric acid. The detailed mechanism for functionalization is reported in our previous publication [10]. Post-functionalization, the various carbons were washed thoroughly with deionized water and dried overnight in a convection oven at 60–70 °C. BET surface areas for acid-treated CNF was calculated to be 127 $m^2\,g^{-1}$ while the corresponding values for the activated carbons were 928 $m^2\,g^{-1}$ (SX Ultra Cat), 881 $m^2\,g^{-1}$ (SX Plus Cat), and 931 $m^2\,g^{-1}$ (DLC Supra 50), respectively [10]. The functionalized CNF were therefore categorized as a lower surface area carbon support while the activated carbon grades fell under the category of higher surface area carbon support.

Table 1
Physical properties of 'as-received' activated carbon grades (datasheet supplied by Norit Inc., Marshall, TX)

| | SX Ultra Cat | SX Plus Cat | DLC Supra 50 |
|---|---|---|---|
| BET surface area ($m^2\,g^{-1}$) | 1300 | 1100 | 2090 |
| Apparent density ($kg\,m^{-3}$) | 280 | 380 | 385 (tamped) |
| Particle size | | | |
| *d*10 (μm) | 3 | 4 | 3–5 |
| *d*50 (μm) | 15 | 29 | 9–13 |
| *d*90 (μm) | 100 | 97 | 50 |

### 2.3. Platinum deposition on functionalized carbon

For platinum deposition, a precursor complex-hydrogen hexachloroplatinate or chloroplatinic acid ($H_2PtCl_6{\cdot}6H_2O$, Aldrich) was chemically reduced to colloidal platinum, which was then adsorbed onto the functionalized carbon surface. The '*polyol*' route [19] of supported catalyst synthesis was employed for the colloidal reduction. The detailed procedure for platinum deposition is elucidated in our previous publication [10]. Platinum content on various carbons (wt%) was determined using a thermogravimetric analyzer (TGA; TGA-SDTA 851e, Mettler-Toledo Instruments). Weight of the residue left after heating the samples to 1100 °C at a rate of 20 °C $min^{-1}$ under air flow was approximated as the platinum content. The average platinum content determined by TGA is shown in Table 2 and compared with Pt content determined for the commercially available supported catalyst – Pt on Vulcan XC-72 carbon obtained from E-TEK Inc., Somerset, NJ. The typical BET surface area for Vulcan XC-72 carbon is roughly 250 $m^2\,g^{-1}$ [20]. In the context of this study, when compared to the activated carbons, Vulcan XC-72 can also be regarded as a lower surface catalyst support, similar to CNF.

#### 2.3.1. Electrochemical characterization of supported catalyst-ESA and ORR activity

Rotating disk electrode (RDE) studies were carried out to determine intrinsic activity of the supported platinum catalyst. The sample preparation stage was similar to the process outlined by Paulus et al. [21]: 10 mg of the supported catalyst was ultrasonically blended with 5 ml deionized water (Millipore SuperQ

Table 2
Platinum content (average wt%) of various supported catalyst systems

| Pt/CNF | Pt/SX Ultra Cat | Pt/SX Plus Cat | Pt/SX DLC Supra 50 | Pt/Vulcan XC-72(E-TEK) |
|---|---|---|---|---|
| 19 | 24 | 22 | 15 | 20 |

System; resistivity 18 MΩ cm), 5 ml of isopropanol and 40 μl of 5% Nafion solution (Fluka) for 15 min. Thereafter, 20 μl of the homogenized solution was pipetted onto a 5 mm diameter glassy carbon disk electrode (glassy carbon area: 0.196 $cm^2$) and allowed to dry in air. Calculations yielded a platinum loading of 21–22 μg $cm^{-2}$ on the glassy carbon disk. The Pt loading was kept constant on the disk for all samples in order to facilitate a fair comparison of the catalytic activity on various carbons.

The glassy carbon disk was next immersed in $N_2$ deaerated electrolyte (0.5 M $H_2SO_4$) and used as the working electrode (WE) in a standard three-electrode set up. A Luggin capillary with a platinum gauze over which hydrogen was produced served as the reversible hydrogen electrode (RHE) or the reference electrode (RE). A platinum wire in fritted glass tube was used as the counter electrode (CE). The working electrode potential was cycled several times between 0.045 and 1.2 V to remove contamination and oxide formation from the WE surface. Room temperature cyclic voltammograms were thereafter measured between 0.4 and 1.2 V (vs. RHE) at a scan rate of 20 mV $s^{-1}$. For ORR measurements, the electrolyte was saturated with pure oxygen for 20 min prior to every run and linear-sweep scans were performed on the disk 0.3 and 1.2 V at a scan rate of 20 mV $s^{-1}$ under oxygen blanket. The disk currents were measured using a bipotentiostat (Pine Instruments). The ORR runs were performed at disk rotation speeds of 400, 625, 900, 1225 and 1600 rpm, respectively.

### 2.4. Electrode preparation from supported catalyst

Using the supported catalyst samples, electrode 'inks' were prepared via the well-known Los Alamos method [22,23]. A representative ink mixture contained the supported catalyst, Nafion® 117 solution (5 wt% in alcohol mixture, Fluka), glycerol and 1 M Tetrabutyl ammonium hydroxide (TBAOH) in alcohol mixture (Fluka). A 5:2 weight ratio was maintained between the supported catalyst and Nafion solution. TBAOH added was equivalent to 5% by weight of Nafion. Additional glycerol was added (if the mixture became too thick and viscous) with the total addition not allowed to exceed 1.2 times the weight of added Nafion solution. The mixture was stirred in a glass vial till a homogeneous ink resulted. Using a paint brush, thin layers of the ink were then painted onto one square side of double-sided poly (tetrafluoroethylene)-PTFE coated decals (area: 5 $cm^2$). Prior calculations dictated the weight of ink required to be painted on the decals to obtain a Pt loading of 0.3 mg $cm^{-2}$. After each coating, the decals were dried in a vacuum oven at 210 °C for 20 min and weighed. The process of painting and drying in the oven was repeated till the desired ink weight was achieved. Platinum loadings for both the cathodes and anodes were kept equivalent.

#### 2.4.1. Measurement of electrical conductivity of carbon support

To determine the electrical conductivity of the supported catalyst, the inks prepared were smeared onto a specially fabricated ceramic substrate (10 mm × 12 mm) with etched gold contacts, Fig. 1(a). Fig. 1(b) shows the substrate with the catalyst ink painted onto its surface. The height of the catalyst ink raised against the ceramic surface (catalyst layer thickness) and catalyst layer width were measured by SEM. Also the spacing between the gold contacts could be easily measured for conductivity calculations. The electrical resistance between any two pins was then measured by a two-probe technique using a digital multimeter (Keithley Instruments Model 2000) with data readback capability. An average value of resistance was calculated based on 25 measurements. Knowing the resistance and the dimensional parameters, average electrical resistivity and conductivity was calculated for each supported catalyst ink.

### 2.5. Fabrication of membrane electrode assembly

A perfluorosulfonic acid ionomer, Nafion® 115 (average thickness: 120 μm) obtained from Ion Power Inc., New Castle, DE was employed to fabricate MEAs. Prior to MEA preparation, the 50 $cm^2$ square membrane pieces were first boiled in 5% $H_2O_2$ and thereafter 0.5 M $H_2SO_4$. Such a process removed organic and inorganic impurities from the surface of the membrane. Subsequently, the membrane pieces were ion-exchanged to $Na^+$ form overnight in a dilute solution of $Na_2SO_4$. The sodium form has superior thermal stability to withstand the hot press procedure employed in adhering electrodes to the membrane [22,24].

Each piece of membrane was subsequently sandwiched between two painted decals (cathode and anode) and hot-pressed

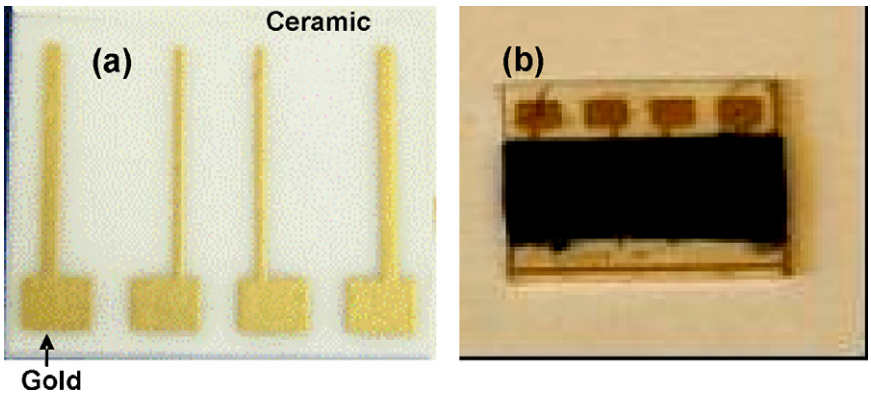


Fig. 1. Ceramic substrate used for electrical resistance measurement of supported catalyst ink (left); substrate painted with supported catalyst ink (right).

for 3 min under at 398 K under 5000 pounds of pressure. This process transferred the ink from decal to the membrane. Decal backings were then peeled off and the MEAs reconverted to their protic forms by boiling in 0.5 M sulfuric acid for 2 h and subsequently dried.

### 2.6. Membrane electrode assembly testing

#### 2.6.1. Fuel cell performance evaluation

For electrochemical performance testing, each MEA was assembled along with PTFE-coated fiberglass gaskets and 5 $cm^2$ gas diffusion layers (GDL) (ELAT® high pressure GDL) in a single cell test fixture with stainless steel end plates and graphite collector channels. The single cell was then connected to a fuel cell test station (FCT 2000, Fuel Cell Technologies Inc., Albuquerque, NM) coupled to a load box (Agilent Technologies, 6063 B, 250 W, 0–10 A, 3–240 V) and interfaced with a computer through a National Instruments LabVIEW program. The test station was equipped with temperature control of the reactant gases and the cell hardware. Inlet gases to the cell were humidified by passing through bubblers containing water and their flow rates controlled using mass flow controllers. Backpressure regulators on the anode and cathode lines allowed regulation of inlet gas pressure.

Temperatures for the inlet fuel-hydrogen at the anode and cathode oxidant (air or oxygen), as well as temperature of the humidifiers, was set at 85 °C. Gas flow rates at both cathode and anode lines were maintained at 100 sccm; the temperature of the cell hardware was held at 80 °C. Regulating the back pressure valves a backpressure of 15 psi (1 atm) was applied to both inlet fuel lines. The cell was maintained at open-circuit or no load conditions until the above mentioned temperature and pressure parameters were attained. Thereafter, a load of 0.6 V was applied to the cell from the loadbox and the measured current allowed to stabilize. Reproducible *V–I* characteristics of the MEA were subsequently measured in the form of galvanodynamic polarization curves with data points recorded at current intervals of 50 mA.

#### 2.6.2. Cell resistance–electrochemical impedance spectroscopy (EIS)

After each polarization curve measurement, cell resistances were measured at open circuit conditions using a bipotentiostat (SI 1280B, Electrochemical Measurement Unit, Solartron Instruments, UK). The reference and working leads of the bipotentiostat were connected to the cathode while the counter lead was connected to the anode. A 10 mV sine wave was applied and the response measured as a Nyquist plot over the range of frequencies—20 MHz to 50 mHz. High frequency intercept of the Nyquist curve on the real axis was approximated as the overall cell resistance and normalized to active area (5 $cm^2$) of the MEA.

#### 2.6.3. Electrochemically active surface area measurement for MEAs

*In situ* electrochemically active surface areas were determined for the MEAs by CO-stripping voltammetry using the bipotentiostat at same temperature and pressure conditions as the polarization measurements. The method followed was similar to Dinh et al. [15]; however in our work, the cathode lead of the fuel cell was connected to the working electrode of the bipotentiostat while anode was used as both a counter electrode and reference electrode due to the negligible overpotential of the hydrogen oxidation reaction (HOR) at the anode. The anode and cathode faces of each MEA were exposed to humidified hydrogen and nitrogen, respectively, at zero back pressures till the open circuit voltage dropped to about 0.1 V. Thereafter, a constant potential of 0.05 V (vs. the hydrogen reference electrode) was set and the cathode gas switched to CO (50 ppm in nitrogen-Praxair) at zero back pressure. Flow of CO continued for approximately 45 min to obtain monolayer coverage on the available platinum sites in the cathode. Prior to CO-stripping, gas flow on the cathode side was switched back to nitrogen for 30 min in order to purge the lines clear of CO. CO-stripping voltammograms were then measured in the potential window of 0.05 and 1.2 V (vs. RHE) at a scan rate of 5 mV $s^{-1}$. Area under the CO-stripping peak for the first cycle was integrated to obtain the couloumbic charge. The ESA was calculated and expressed in $m^2$ per unit weight of platinum catalyst in the MEA.

## 3. Results and discussion

### 3.1. Electrochemical characterization of supported catalysts

#### 3.1.1. CV and ESA determination

A comparison of cyclic voltammograms for the supported catalyst systems is presented as a plot of mass activity (current per unit weight of catalyst) against the potential in Fig. 2. Well-defined hydrogen adsorption/desorption features are evident for most of the catalyst systems. Curves for the activated carbons indicated as (b), (c) and (d) in Fig. 2 exhibit a very strong capacitive current in the double layer charging region

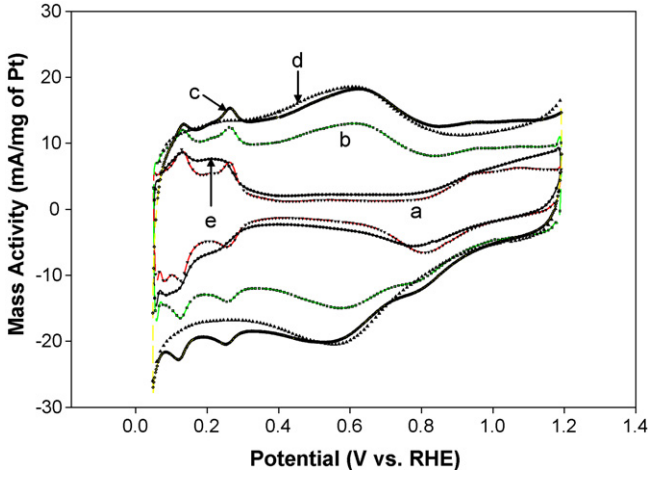


Fig. 2. Cyclic voltammograms of various carbon supported platinum systems in 0.5 M $H_2SO_4$ solution at room temperature at a scan rate of 20 mV $s^{-1}$: (a) Pt/CNF, (b) Pt/Ultra Cat, (c) Pt/Plus Cat, (d) Pt/DLC Supra 50 and (e) Pt/Vulcan XC-72 (E-TEK).

Table 3
Electrochemically active surface area (ESA) of various supported catalyst systems as determined by hydrogen adsorption–desorption cyclic voltammetry

| Catalyst | Pt loading ($\mu g\,cm^{-2}$) | ESA ($cm^2$) | ESA ($m^2\,g^{-1}$ of Pt) |
|---|---|---|---|
| Pt/CNF | 22.0 | 1.7 | 40.5 |
| Pt/Ultra Cat | 23.0 | – | – |
| Pt/Plus Cat | 22.0 | – | – |
| Pt/DLC Supra 50 | 21.5 | – | – |
| Pt/Vulcan XC-72 (E-TEK) | 21.1 | 1.9 | 45.4 |

The ESA values for the Ultra Cat, Plus Cat and DLC SUPRA 50 carbons could not be determined due to large double layer charging.

(0.4–0.6 V vs. RHE). The double layer charging is not surprising, considering the high surface areas of the activated carbon supports [25] (Table 1). The adsorption/desorption peak currents for the activated carbons are much larger than those for CNF and Vulcan XC-72 carbon, however, these currents includes a significant contribution from current due to double layer charging on the higher surface area AC, making it quite difficult to accurately determine the charge under the hydrogen adsorption/desorption region. Voltammograms for the lower surface area supports-CNF and Vulcan XC-72 carbon overlap each other and exhibit a much lower capacitive current compared to the activated carbons. ESA of platinum on various carbons is estimated by integrating charge under the hydrogen adsorption region of the voltammogram and is normalized to the platinum content on the glassy carbon disk. Incorporating a value of $210\,\mu C\,cm^{-2}$ for adsorption/desorption of a hydrogen monolayer on a smooth platinum surface [26], the ESA was calculated using the following expression [27]:

$$\text{ESA}\,(\text{cm}^2\,\text{g}^{-1}\,\text{Pt}) = \frac{\text{charge}\,(\mu\text{C}\,\text{cm}^{-2})}{210\,(\mu\text{C}\,\text{cm}^{-2}\,\text{Pt}) \times \text{Pt loading}\,(\text{g}\,\text{Pt}\,\text{cm}^{-2})} \quad (1)$$

The ESA values could be determined only for CNF and Vulcan XC-72 and are tabulated in Table 3. The activated carbons on the other hand, do indicate active platinum facets on their surface, however the large capacitive current due to double layer charging, which increases with increasing surface area of the support, makes determination of ESA extremely difficult.

### 3.1.2. Oxygen reduction activity of Pt/C catalysts

The RDE cathodic curves in Fig. 3 indicate measured current density at various potentials for the supported catalyst systems at a disk rotation speed of 1225 rpm. For sake of clarity, Fig. 3(a) compares Pt/CNF with Pt/Vulcan XC-72 while the activated carbon supported catalyst systems are compared in Fig. 3(b). From the curves, the oxygen reduction reaction is under mixed kinetic and diffusion control in the potential range of 0.9 and 0.6 V followed by a purely diffusion-limited region below 0.6 V. To eliminate the diffusion effect and obtain purely kinetic current, the ORR curves in Fig. 3 were corrected using the

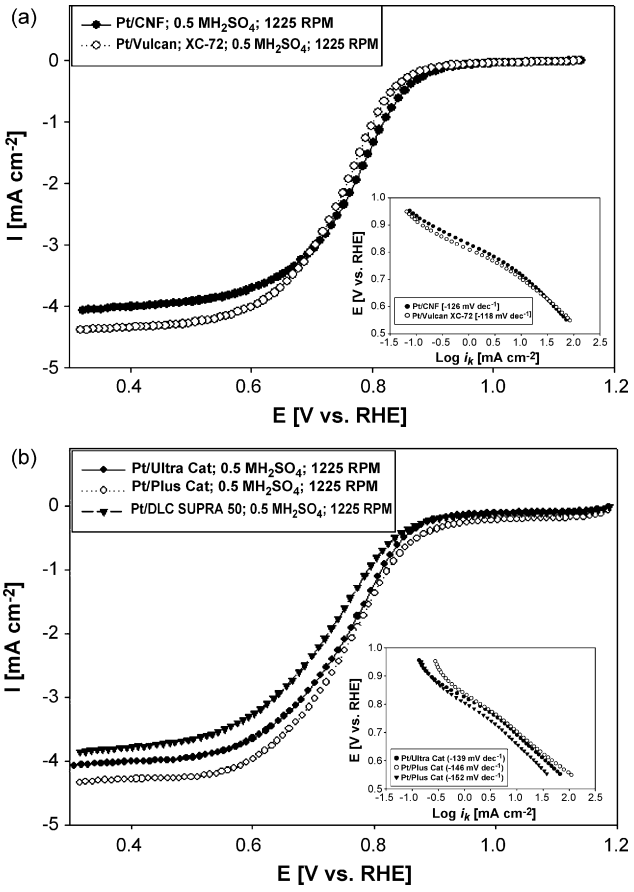


Fig. 3. Disk currents obtained on the various supported catalysts during ORR in the cathodic sweep at scan rate of 20 mV $s^{-1}$, electrolyte is 0.5 M $H_2SO_4$ and data is presented for cathodic sweep at a disk rotation rate of 1225 rpm: (a) Pt/CNF and Pt/Vulcan XC-72 (E-TEK); (b) Pt/Ultra Cat, Pt/Plus Cat and Pt/DLC Supra 50. Figures in inset indicate Tafel plots—potential vs. mass transport corrected kinetic currents ($I_k$).

expression [28]:

$$I_k = \frac{I_L I}{I_L - I} \quad (2)$$

where $I_k$ is the purely kinetic (diffusion free) current, $I_L$ is the mass-transport limiting current or Levich current, and $I$ is the measured current. This equation is valid on a smooth electrode when the ORR obeys first-order kinetics. The limiting currents measured at 0.3 V were found to be in good agreement with the Levich equation with a linear relationship obtained between $I_L$ and $\omega^{1/2}$ where $\omega$ is the disk rotation speed in rad $s^{-1}$ [29]. Inset images in Fig. 3 are the semi-logarithmic Tafel plots – potential against diffusion corrected currents. From the Tafel plots, the slope of the curve, or the Tafel slope was established. Table 4 highlights the Tafel slopes and kinetic currents determined for the various samples.

The kinetic currents were found to be similar among the low surface area carbons—CNF and Vulcan, and among the higher surface area activated carbons, with the exception of the highest surface area-DLC grade. The intrinsic Tafel slopes for ORR were also close to each other, ranging from $-118\,mV\,dec^{-1}$ to $-152\,mV\,dec^{-1}$ at room temperature (Table 4). From Fig. 3(a)

Table 4
Kinetic parameters for various supported catalysts as determined by RDE experiments carried out in 0.5 M $H_2SO_4$ saturated with oxygen at room temperature

| Catalyst | $b$ (mV dec$^{-1}$) | $I_k$ @ 0.8 V (mA cm$^{-2}$) |
|---|---|---|
| Pt/CNF | −126 | 1.98 |
| Pt/Ultra Cat | −139 | 1.53 |
| Pt/Plus Cat | −146 | 1.99 |
| Pt/DLC Supra 50 | −152 | 1.02 |
| Pt/Vulcan XC-72 (E-TEK) | −118 | 1.42 |

Data reported for a disk rotation speed of 1225 rpm.

and (b), even though the Tafel slopes appear to be changing from lower overpotential region (>0.85 V) to higher overpotential regions (<0.85 V), the calculated values did not differ significantly, hence a single slope is reported. This is contrary to the observations made by observed by Paulus et al., where the Tafel slope varied from −60 mV dec$^{-1}$ at low overpotentials to −120 mV dec$^{-1}$ at higher overpotentials [21]. When plotted together, the Tafel curves overlapped each other, thus suggesting that the relative catalytic activity of platinum on the various carbons is very similar, as are the exchange current densities for the various supported catalysts. The similarities in the ESA values and the near identical Tafel curves lead us to believe that for the supported catalyst systems studied and the catalyst loadings employed, the choice of support and its electrochemical properties do not significantly affect the catalyst activity in the kinetic region. The randomness in the kinetic current values points in the same direction. Purely based on Tafel slopes among those studied, the lower surface area carbons appear to be slightly preferable and independent of the support morphology (i.e. fibers for nanofibers vs. agglomerated spheres for the activated carbon).

### 3.2. MEA performance measurement

Electrochemical performance of MEAs fabricated from the supported catalyst systems are compared as *V–I* polarization curves in Fig. 4. The MEAs were tested in a fuel cell using hydrogen as the anode fuel and air (Fig. 4(a)) and oxygen (Fig. 4(b)) as the cathode feed. The polarization curves for each of the fabricated MEAs were measured under strictly comparable conditions. MEA fabricated from the E-TEK catalyst using the same method was tested as a benchmark comparison.

Both sets of polarization curves in Fig. 4 indicate significant activation overpotential below 'open-circuit' conditions. Comparing Fig. 4(a) with (b), the fuel cell performance is understandably better (i.e. higher voltage at any given current density) when oxygen is the oxidant instead of air. Also a comparison of the curves in air and oxygen reveals that the polarization response of the CNF MEA is clearly superior to the three activated carbon MEAs and comparable to the E-TEK MEA. Among the activated carbons, fuel cell performances of the two predominantly mesoporous grades-SX Ultra Cat and SX Plus Cat are similar to each other, while the MEA fabricated from the predominantly microporous DLC Supra 50 grade exhibits the worst performance with a sharp drop beyond open circuit voltage. The limiting current density values are close for the two lower surface area carbons while the higher surface area activated carbons show a much lower value.

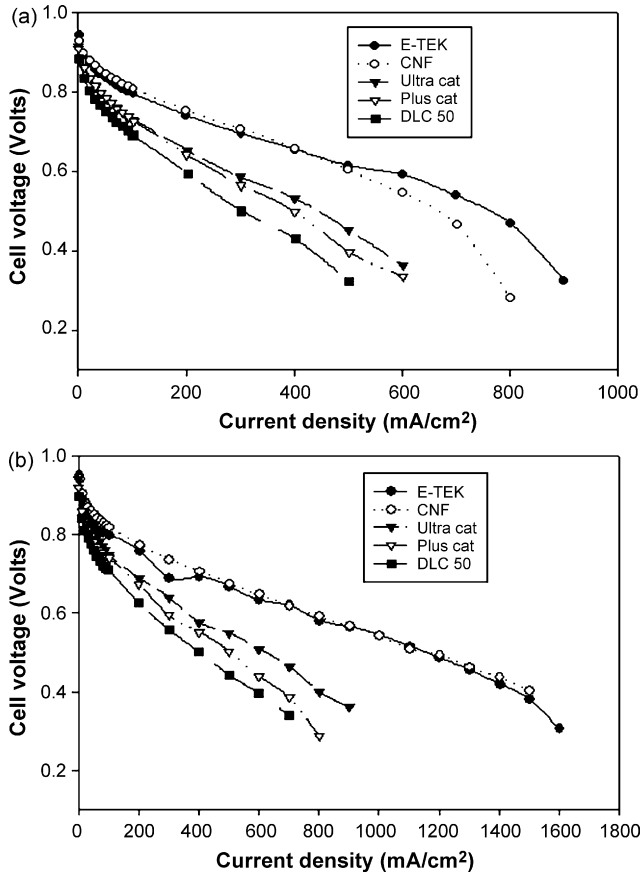


Fig. 4. Cell polarization curves for MEAs prepared using different supported catalysts. Anode fuel-$H_2$, cathode oxidant: (a) air and (b) oxygen. Platinum catalyst loading on anode and cathode is 0.3 mg cm$^{-2}$. Membrane: Nafion® 115. Operating conditions: $T_{Cell} = 80\,^{\circ}C$, $T_{Humidifier\ (cathode\ and\ anode)} = 85\,^{\circ}C$, $backpressure_{(cathode=anode)} = 15$ psi.

### 3.3. Determination of cell resistance

Beyond the kinetic region (150–200 mV below open circuit), the almost linear drop in the voltage corresponds to the ohmic overpotential or losses due to ohmic resistance to the flow of protons (through the membrane) and electrons through the MEA hardware, current collector plates and the external leads of the circuit. Also contributing to the voltage drop is contact resistance in the external circuit and interfacial resistance among various components of the fuel cell assembly [30]. Electrochemical impedance spectroscopy was used to determine the values of cell resistance. The data is in the form of a Nyquist plot, where the real component of impedance ($Z'$) is plotted against the imaginary component ($Z''$). A typical Nyquist plot for the Ultra Cat carbon MEA measured under open circuit conditions is shown in Fig. 5. Cell resistances were obtained from the value of intersection at high frequency with the real axis, where the imaginary component is zero. The measured resistance (in Ω) normalized to geometric area of the electrode in the MEA gives the resistance in Ω cm$^2$.

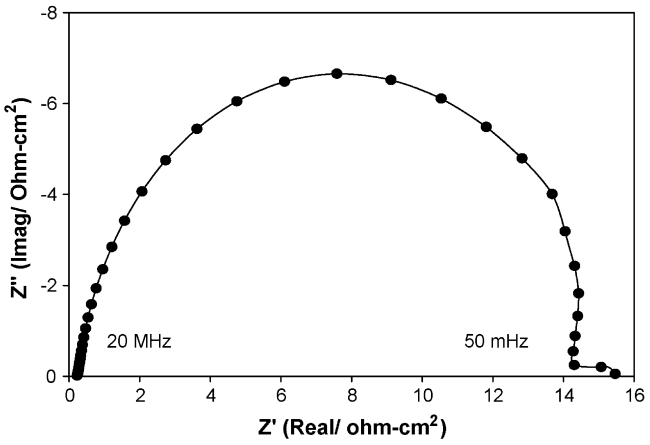


Fig. 5. Nyquist plot for Ultra Cat MEA (Pt loading on cathode and anode: 0.3 mg cm$^{-2}$) at an applied potential equivalent to the open circuit voltage conditions, frequency range: 20 MHz to 50 mHz, amplitude: 10 mV.

Voltage at 400 mA cm$^{-2}$ determined from MEA polarization curves and the average resistance values determined by EIS are tabulated in Table 5. Comparing the data in Table 5 with the polarization curves in Fig. 4, the superior performance of CNF MEA in the ohmic region over the activated carbon MEAs is attributed in part to its lower $R$ value. Also from Table 5, we can conclude that the comparable performances of the CNF MEA with E-TEK MEA (as evident from the polarization curves) correlate with similar $R$ values as well. It is well-known that the major component of overall cell resistance is the membrane resistance. The membrane used in this work (Nafion® 115) was common to all the MEAs fabricated from the various carbons and, to a first approximation, would have a fixed resistance value under similar conditions of MEA assembly and testing. A reported value of the area specific ohmic resistance of humidified Nafion® 115 at 80 °C under very similar conditions of single fuel cell testing is ca. 0.125 Ω cm$^2$ [31].

The observed difference in the $R$ values among the various MEAs is therefore a result of other factors specific to our preparation and testing methods. These factors include contact resistances at various interfaces, cell hardware resistance and electrical resistance through the leads. The amorphous Vulcan carbon support in the E-TEK MEA is inherently known to be less conductive than the graphitic CNF, yet its MEA performance is similar to CNF. This result suggests that for the platinum loadings employed in our work, neither the type of lower surface area support used (CNF or Vulcan) nor its morphology (fibrular for CNF and spherical for Vulcan) has a significant bearing on the MEA performance in a fuel cell. It is also possible that the electrode material has an impact on membrane hydration. The high surface area carbon may adsorb more water, keeping the membrane dry, or may present a more compact morphology, limiting water transport into the membrane.

Table 5
Electrochemical performance parameters obtained for various MEAs from polarization curves in Fig. 4 and from EIS measurements on the MEAs

| MEA | Cell reactants | Voltage @ 400 mA cm$^{-2}$ (V) | Average resistance, $R$ (Ω cm$^2$) |
|---|---|---|---|
| CNF | $H_2$/air | 0.66 | 0.21 |
| Ultra Cat | $H_2$/air | 0.53 | 0.35 |
| Plus Cat | $H_2$/air | 0.50 | 0.37 |
| DLC Supra 50 | $H_2$/air | 0.43 | 0.40 |
| E-TEK | $H_2$/air | 0.66 | 0.21 |
| CNF | $H_2/O_2$ | 0.71 | 0.23 |
| Ultra Cat | $H_2/O_2$ | 0.58 | 0.29 |
| Plus Cat | $H_2/O_2$ | 0.55 | 0.39 |
| DLC Supra 50 | $H_2/O_2$ | 0.50 | 0.39 |
| E-TEK | $H_2/O_2$ | 0.69 | 0.22 |

Such a water management problem can very likely occur in the AC MEAs wherein the highly porous, carbon support surface gets inundated with water at higher current densities. This may explain the drastic performance drop observed in the polarization curves for the activated carbons and the lowering of limiting current densities, as opposed to the lower surface area carbons. This problem is less likely to occur in lower surface area carbons such as the Vulcan XC-72 and non-porous carbons such as CNF. There is therefore a threshold of carbon surface area beyond which the support surface area starts to adversely affect the fuel cell performance.

### *3.4. Influence of supported catalyst electrode microstructure on fuel cell performance*

As discussed earlier, the cell resistance $R$ obtained from EIS at the high frequency intercept consists of all the ohmic resistances in the cell (electrolyte resistance of the Nafion membrane, some contribution of electrolyte ionic resistance electrolyte in the reaction layer, contact resistances in the single cell, hydrogen polarization losses and some contribution from the mass transport [31,32]. Contact resistances can be further classified into protonic interfacial contact resistance, which is the resistance to the proton transfer at the interface between the catalyst layer, the impregnated Nafion ionomer and the bulk membrane and the electronic contact resistance, which is the resistance of the electrodes, membrane and current collecting components [30]. Electronic contact resistance is a strong function of electronic conductivity of various current collecting components, namely the electrode layer, graphite blocks and end plates, as well as the interfacial contact between the various layers. As discussed earlier, the Nafion® 115 membrane is common to all the MEAs fabricated and tested in this work-under the similar conditions of fuel cell testing employed, the membrane should be well hydrated and therefore, have a very small contribution to the overall cell resistance.

Thus, the fuel cell performance loss in the ohmic region may be a consequence of the electronic contact resistances in cell and the conductivity of the electrode layer. In order to further investigate the influence of contact resistance, microstructural features of various supported catalyst ink painted decals (electrodes) were inspected by SEM. A comparison of SEM micrographs in Fig. 6. clearly shows the difference in surface morphologies of various electrodes. It must be noted that the surfaces imaged are those which eventually come in contact with the membrane within the MEA. The E-TEK electrode displays a smooth, almost planar surface while the CNF electrode surface

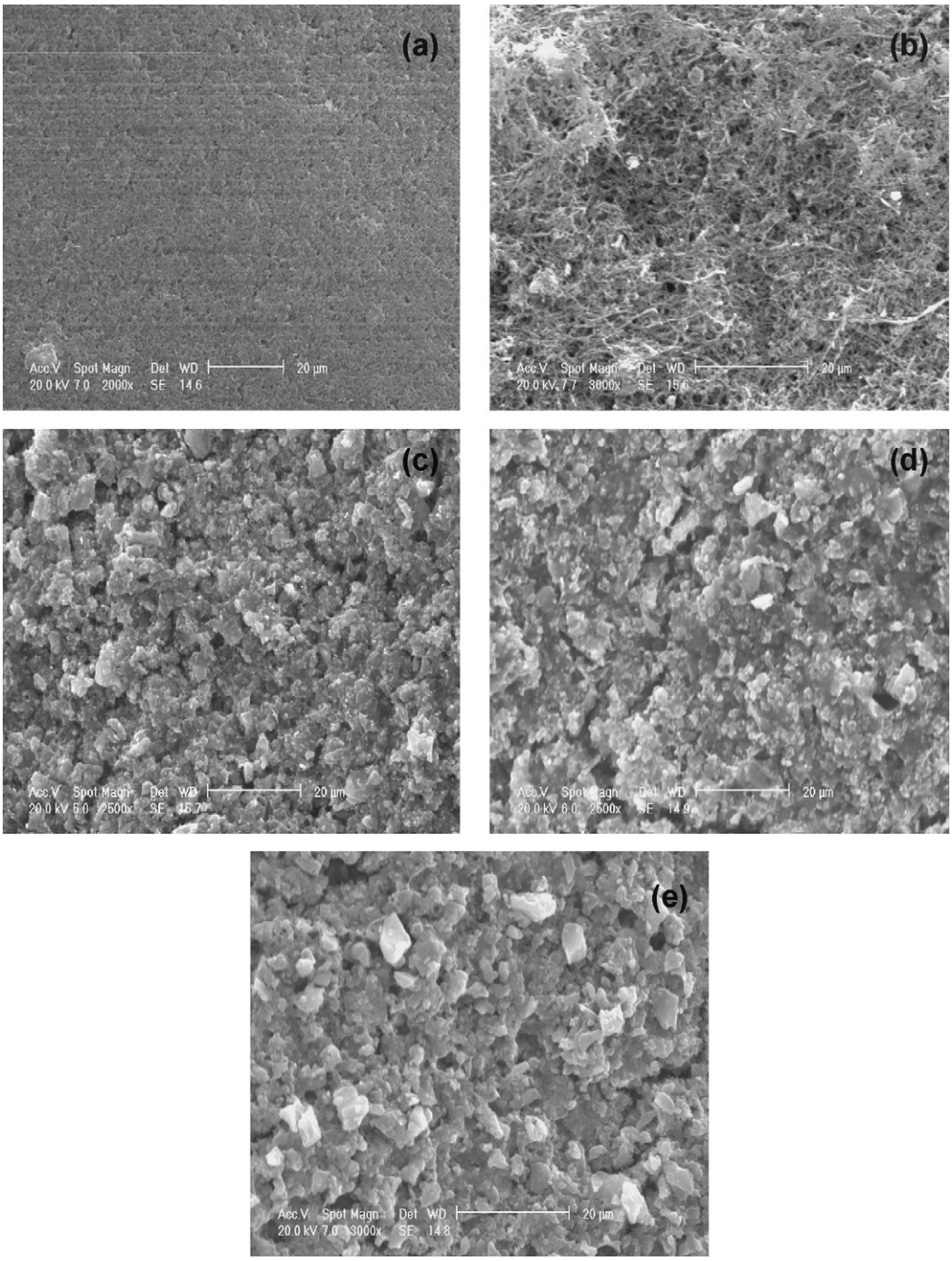


Fig. 6. SEM images of the surface microstructure of fuel cell electrodes prepared using various carbons: (a) Vulcan XC-72 (E-TEK), (b) CNF, (c) SX Ultra Cat, (d) SX Plus Cat and (e) DLC Supra 50.

is very fibrous with an almost mesh-like morphology. The activated carbon electrode surfaces on the other hand are very rough, uneven and filled with cracks, pores and crevices. Comparing the SEM images with the cell resistance values obtained from EIS in Table 5, the lower cell resistances obtained for the E-TEK and CNF electrodes can be attributed, in part, to the good interfacial contact between the electrode and the Nafion membrane due to their smooth planar surface. As the electrode surface becomes coarser, as with the activated carbon MEAs, the interfacial contact worsens leading to high contact resistance. The microstructure of the electrode also affects the mass transport of the fuel through the electrode with a lower value of diffusion resistances obtained for a smoother electrode surface than a coarser one [33].

Fig. 7 shows the cross-sectional SEM images of the MEAs fabricated using the various carbons. It is clear from the SEM images that for the E-TEK and the CNF MEAs, the interfacial contact is good, as indicated by the smoothness of the membrane–electrode layer interface and absence of surface delamination. This planar surface aids in the formation of better

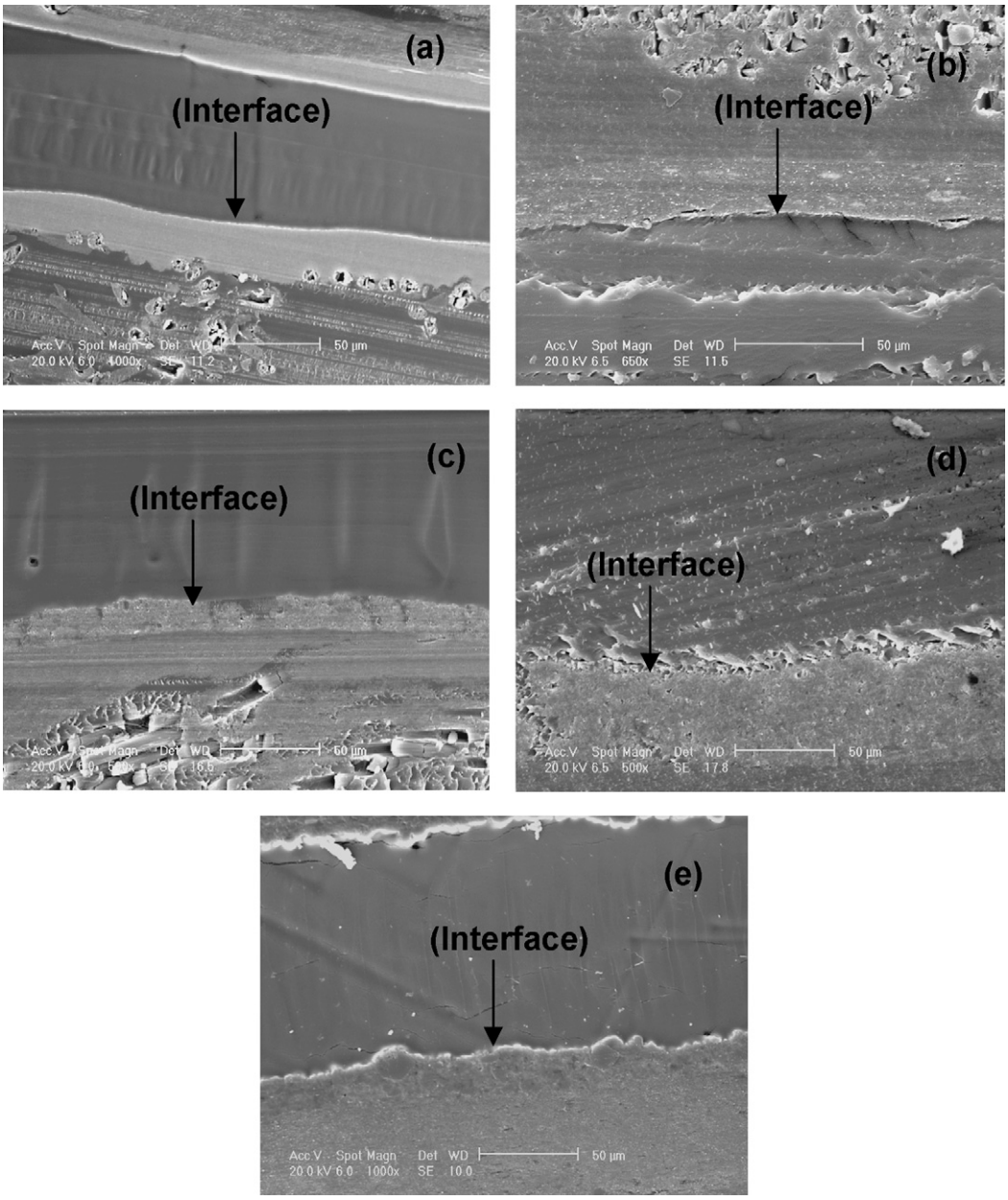


Fig. 7. Cross-sectional SEM images of MEAs prepared using various carbons: (a) Vulcan XC-72 (E-TEK), (b) CNF, (c) SX Ultra Cat, (d) SX Plus Cat and (e) DLC Supra 50. Arrow indicates the boundary between the electrode and the Nafion® 115 membrane.

interfacial contact between the catalyst layer and the ionomeric membrane. As result of a smoother interface, the contact resistance in the MEA which is one of the factors that leads to fuel performance drop in the ohmic region, is reduced.

### 3.5. ESA of platinum in MEA

Carbon monoxide stripping or CO-stripping cyclic voltammetry has been frequently used for *in situ* determination of the ESA within a MEA [12–15]. A representative CO-stripping voltammogram for the E-TEK MEAs is illustrated in Fig. 8. The charge under the CO-stripped region, after the second cycle was determined and assuming a value of 484 $\mu C\,cm^{-2}$ for adsorption/desorption of a monolayer of CO on a smooth platinum surface [34], the ESA was calculated using the following expression [27]:

$$\text{ESA}\,(\text{cm}^2\,\text{g}^{-1}\,\text{Pt}) = \frac{\text{charge}\,(\mu\text{C}\,\text{cm}^{-2})}{484\,(\mu\text{C}\,\text{cm}^{-2}\,\text{Pt}) \times \text{Pt loading}\,(\text{g Pt}\,\text{cm}^{-2})} \quad (3)$$

The ESA values (in $cm^2$ and $m^2\,g^{-1}$ of Pt) are highlighted in Table 6. Table 6 also compares ESA with the mean surface area (MSA) calculated based on the average platinum particle sizes on various carbon supports determined by XRD [10]. The MSA ($m^2\,g^{-1}$ of Pt) is calculated using Eq. (4) assuming the platinum

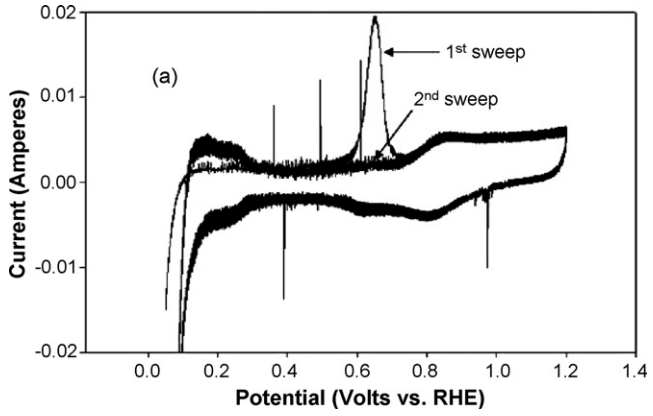


Fig. 8. CO-stripping voltammogram indicating the first and second sweeps at 5 mV $s^{-1}$ between 0.05 and 1.2 V for the E-TEK MEA. CO adsorption from 50 ppm CO in $N_2$ took place at 0.05 V for 45 min.

particles deposited on various carbons to be spherical [11]:

$$\mathrm{MSA} = \frac{6000}{\rho L} \tag{4}$$

where $\rho$ is the density of bulk platinum (21.4 g $cc^{-1}$) and $L$ is the average particle diameter calculated for various supported catalyst systems in our previous work [10]. The ratio between ESA and MSA indicates the percentage of the available platinum surface 'active' for catalysis. From Table 6, it can be seen that E-TEK MEA has the best availability of electrochemically active Pt surface, followed by Plus Cat, Ultra Cat, CNF and DLC Supra 50, respectively. One observation that is clear from the Pt area utilization comparison is that a high surface area available on the support (such as in the case of the activated carbons) does not ensure a greater availability of active platinum surface for catalysis. From Table 6, the activated carbon grades, in spite of their large surface areas, utilize electrochemically at best only a 13% of the platinum surface area available. Also, the trend in platinum utilization area displayed by the MEAs does not mirror the corresponding polarization curve trends. Thus, again for the carbons utilized in this work, the overall fuel cell performance of the corresponding MEA is strongly governed by material characteristics such as surface microstructure and nature of electron transport, and not just the fraction of electroactive platinum available. Fuel cell performance of the CNF closely follows that of the E-TEK despite the E-TEK MEA having almost thrice the platinum area accessible for catalytic activity (as determined by CO-stripping voltammetry), which further reiterates the weak dependence of MEA performance on the nature of the support for low surface area carbons such as CNF and Vulcan carbon.

### 3.6. Electrical resistivity of supported catalyst

To investigate the influence of catalyst support conductivity on the overall fuel cell performance, electrical resistance of the supported catalyst was measured. SEM micrographs of the various inks painted on the ceramic substrate for conductivity measurements are shown in Fig. 9(a–e). Average ink thickness, measured electrical resistance and the calculated values of electrical resistivity and conductivity are indicated in Table 7. Clearly, the trend in the measured resistance and calculated resistivity/conductivity values mirrors the relative fuel cell performance in the ohmic drop region of the polarization curves. The superior resistance of the graphitic carbon nanofibers compared to the other carbons is a significantly important factor in this region. This excellent conductivity/low resistivity of the carbon nanofibers makes up for the low utilization of platinum in the corresponding fabricated MEA as compared to the utilization of platinum in the E-TEK MEA. On the other hand, the Vulcan XC-72 carbon displays an order of magnitude higher resistance than the CNF yet its fuel cell performance is at par with the CNF MEA. This observation again reiterates the belief that for the range of Pt loadings employed and the systems tested, the low surface area carbons make no significant contribution to the overall cell performance and can for practical

Table 6
Comparison of ESA (calculated from CO-stripping voltammograms), MSA (calculated for the supported catalysts by XRD) and electrochemical utilization of available platinum area, for various MEAs

| MEA | Average Pt particle size, $L$ [10] (nm) | ESA ($cm^2$) | ESA ($m^2\ g^{-1}$ of Pt) | MSA ($m^2\ g^{-1}$ of Pt) | Pt area utilization (%) |
|---|---|---|---|---|---|
| CNF | 3.5 ± 0.2 | 114.0 | 7.6 | 78.7 | 9.7 |
| Ultra Cat | 3.2 ± 0.2 | 140.6 | 9.4 | 85.9 | 10.9 |
| Plus Cat | 3.4 ± 0.1 | 163.8 | 11.0 | 82.3 | 13.3 |
| DLC Supra 50 | 2.4 ± 0.2 | 121.9 | 8.1 | 113.2 | 7.2 |
| E-TEK | 2.4 ± 0 | 484.2 | 32.3 | 116.4 | 27.7 |

Table 7
Comparison of resistivity and conductivity of various supported catalyst inks coated onto a ceramic substrate etched with gold electrodes

| Catalyst ink | Average ink layer thickness (μm) | Average measured resistance | Average resistivity[a] (Ω cm) | Average conductivity (S $cm^{-1}$) |
|---|---|---|---|---|
| Pt/CNF | 325 | 3.08 Ω | 0.1 | $1 \times 10^{1}$ |
| Pt/Ultra Cat | 138 | 8.54 kΩ | 235.7 | $4.2 \times 10^{-3}$ |
| Pt/Plus Cat | 197 | 5.28 kΩ | 148.6 | $6.7 \times 10^{-3}$ |
| Pt/DLC Supra 50 | 460 | 0.53 MΩ | 48654 | $2.1 \times 10^{-5}$ |
| Pt/Vulcan XC-72 (E-TEK) | 36 | 0.31 kΩ | 11.6 | $8.6 \times 10^{-2}$ |

[a] Through plane resistivity determined based on area calculated using layer thickness, layer width and distance between gold pins.

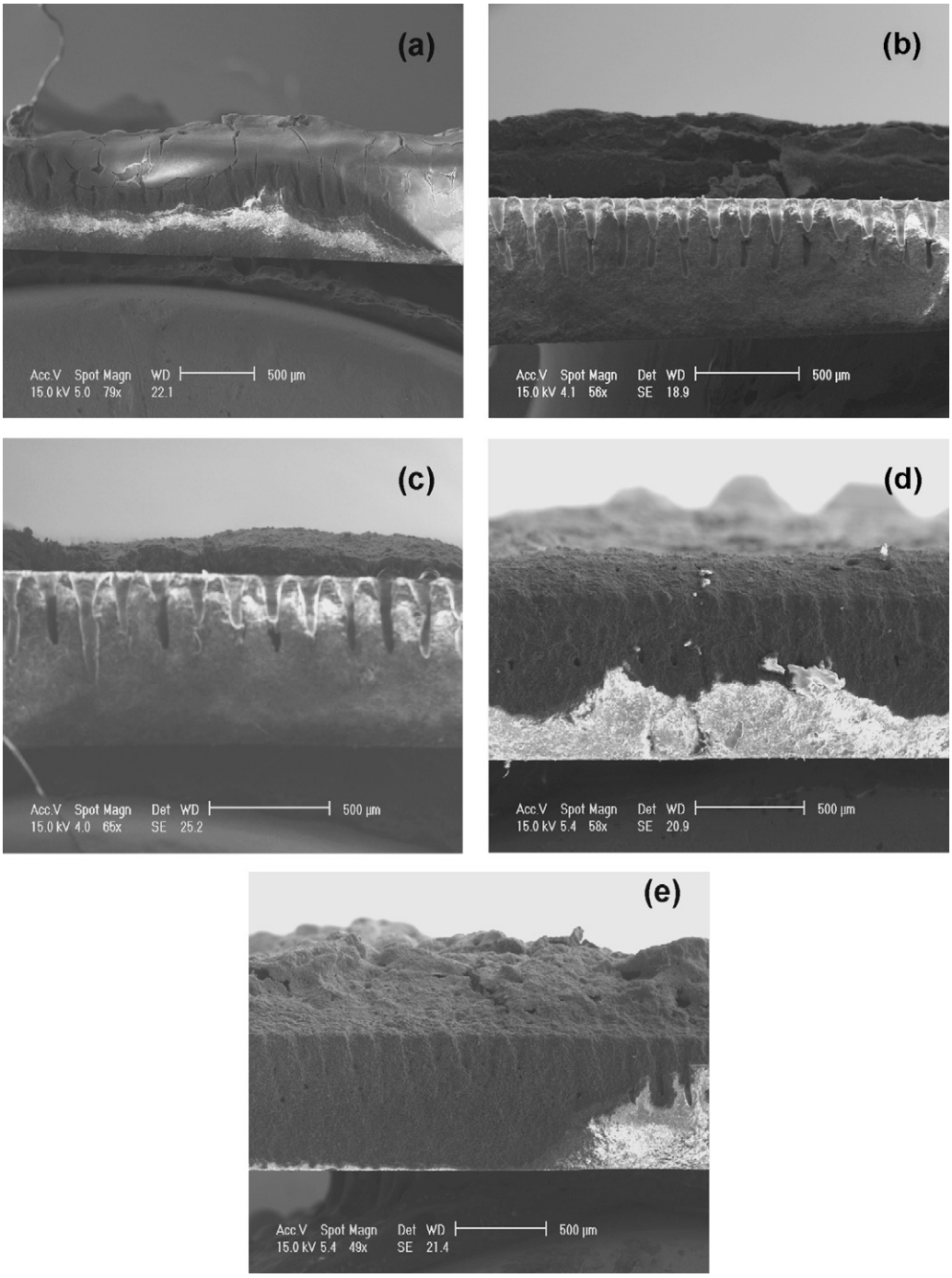


Fig. 9. SEM micrographs of supported catalyst ink coating on ceramic substrate for electrical conductivity measurement: (a) Vulcan XC-72 (E-TEK), (b) CNF, (c) SX Ultra Cat, (d) SX Plus Cat and (e) DLC Supra 50.

applications be interchangeably used. The nanofibers used in fuel cell MEA fabrication thus have potential for reducing cell resistance without sacrificing fuel cell performance. The activated carbons display very poor electrical conductivity which is many orders of magnitude lower than the two low surface area carbons. Thus, for these high surface carbons, the nature of the material surface (conductivity and surface morphology) makes a much more significant contribution to the overall fuel cell performance.

## 4. Conclusions

Catalyst supports such as carbon need to serve the dual purpose of providing high surface area (for catalyst deposition) and superior electrochemical properties-primarily good electronic conductivity. In this work, a comparison of the electrochemical properties of various carbon supported platinum catalyst samples reveals some interesting observations. The supported catalyst (Pt) displays nearly identical catalytic activity in the

'as-prepared' state, being independent of the type of support on which it is deposited (graphitic or amorphous; high surface area or low surface area). When the same supported catalysts are fabricated into MEAs and tested in fuel cell, the carbon support characteristics start to yield a greater influence on the overall fuel cell performance. This behavior is much more prominent for MEAs fabricated from high surface area supports. For these supports, their microstructure, mass-transport properties and electrical conductivity characteristics become very critical to towards the MEA exhibiting acceptable fuel cell behavior. The characteristics of the lower surface area supports such as carbon nanofibers and Vulcan XC-72 carbon do not influence the performance the manner in which the high surface area carbons do, and therefore for all practical purposes the two can be interchangeably used while fabricating MEAs. That being said, superior electrical conductivity does seem to be an important asset for a catalyst support leading to excellent electronic transport through the cell as well as lower contact resistances. The complete analysis of the electrochemical behavior of the support is certainly not complete and would require extensive durability studies such as an investigation into support corrosion and the long term influence of the support on catalyst particle size.

## Acknowledgements

The authors acknowledge the instrumental support provided by the Jesse Wainright group in the Department of Chemical Engineering at Case Western Reserve University. One of the authors (AG) would like to thank Dr. Vivek Srinivasamurthi, former research associate in the Chemical Engineering Department at Case for useful suggestions and constructive guidance.

Pyrograf® is a registered trademark of Applied Sciences Inc., Cedarville, OH, Norit® is a registered trademark of Norit Americas Inc., Marshall, TX; Vulcan® is a registered trademark of Cabot Corporation, Billerica MA; E-TEK$^{sm}$ is a registered service mark of PEMEAS Fuel Cell Technologies—E-TEK Division, Somerset, NJ; E-LAT® is a registered trademark of PEMEAS Fuel Cell Technologies—E-TEK Division, Somerset N and Nafion® is a registered trademark of The E.I. DuPont de Nemours and Company, Wilmington DE.

## References

[1] E. Auer, A. Freund, J. Pietsch, T. Tacke, Appl. Catal. A.: Gen. 173 (1998) 259–271.
[2] F. Rodríguez-Reinoso, Carbon 36 (1998) 159–175.
[3] R. Yu, L. Chen, Q. Liu, J. Lin, K.-L. Tan, S.C. Ng, H.S.O. Chan, G.-Q. Xu, T.S. Andy Hor, Chem. Mater. 10 (1998) 718–722.
[4] B. Xu, X. Yang, X. Wang, J. Guo, X. Liu, J. Power Sources 162 (2006) 160–164.
[5] J. Laramie, A. Dicks, Fuel Cell Systems Explained, second ed., Wiley, England, 2003, p. 6.
[6] M. Eikerling, A.S. Loselevich, A.A. Kornyshev, Fuel Cells 4 (2004) 131–140.
[7] V. Lordi, N. Yao, J. Wei, Chem. Mater. 13 (2001) 733–737.
[8] T.G. Ros, A.J. van Dillen, J.W. Geus, D.C. Koningsberger, Chem. Eur. J. 8 (2002) 1151–1162.
[9] J.P. Chen, S. Wu, Langmuir 20 (2004) 2233–2242.
[10] A. Guha, W. Lu, T.A. Zawodzinski, D.A. Schiraldi, Carbon 45 (2007) 1506–1517.
[11] A. Pozio, M. De Francesco, A. Cemmi, F. Cardellini, L. Giorgi, J. Power Sources 105 (2002) 13–19.
[12] A. Taniguchi, T. Akita, K. Yasuda, Y. Miyazaki, J. Power Sources 130 (2004) 42–49.
[13] S.Q. Song, Z.X. Liang, W.J. Zhou, G.Q. Sun, Q. Xin, V. Stergiopoulos, P. Tsiakaras, J. Power Sources 145 (2005) 495–501.
[14] R.L. Borup, N.E. Vanderborgh, Proceedings of the First International Symposium on Proton Conducting Membrane Fuel Cells, Chicago, IL, 1995, p. 167.
[15] H.N. Dinh, X. Ren, F.H. Garzon, P. Zelenay, S. Gottesfeld, J. Electroanal. Chem. 491 (2000) 222–233.
[16] S.K. Zecević, J.S. Wainright, M.H. Litt, S.L. Gojković, R.F. Savinell, J. Electrochem. Soc. 144 (1997) 2973–2982.
[17] S.L. Gojković, S.K. Zecević, R.F. Savinell, J. Electrochem. Soc. 145 (1998) 3713–3720.
[18] V.S. Murthi, R.C. Urian, S. Mukerjee, J. Phys. Chem. B 108 (2004) 11011–11023.
[19] W.X. Chen, J.Y. Lee, Z. Liu, Chem. Commun. (2002) 2588.
[20] http://www.etek-inc.com/standard/product_NMC.php?prodid=59.
[21] U.A. Paulus, T.J. Schmidt, H.A. Gasteiger, R.J. Behm, J. Electroanal. Chem. 495 (2001) 134–145.
[22] M.S. Wilson, S. Gottesfeld, J. Appl. Electrochem. 22 (1992) 1–7.
[23] M.S. Wilson, Membrane catalyst layer for fuel cells, US Patent 5,211,984 (1993).
[24] S.H. de Almeida, Y. Kawano, J. Thermal Anal. Cal. 58 (1999) 569–577.
[25] A. Essalik, K. Amouzegar, O. Savadogo, J. Appl. Electrochem. 25 (1995) 404–407.
[26] T. Biegler, D.A.J. Raud, R. Woods, J. Electroanal. Chem. Interf. Electrochem. 29 (1971) 269.
[27] T.R. Ralph, G.A. Hards, J.E. Keating, S.A. Campbell, D.P. Wilkinson, M. Davis, J. St-Pierre, M.C. Johnson, J. Electrochem. Soc. 144 (1997) 3845–3857.
[28] J.A. Poirier, G.E. Stoner, J. Electrochem. Soc. 141 (1994) 425–430.
[29] G. Prentice, Electrochemical Engineering Principles, Prentice Hall, New Jersey, 1991, pp. 163–169.
[30] T. Navessin, M. Eikerling, Q. Wang, D. Song, Z. Liu, J. Horsfall, K.V. Lovell, S. Holdcroft, J. Electrochem. Soc. 152 (2005) A796–A805.
[31] F. Liu, B. Yi, D. Xing, J. Yu, H. Zhang, J. Membrane Sci. 212 (2003) 213–223.
[32] S.J. Lee, S. Mukerjee, J. McBreen, Y.W. Rho, Y.T. Kho, T.H. Lee, Electrochim. Acta 43 (1998) 3693–3701.
[33] Z. Wang, Y. Liu, V.M. Linkov, J. Power Sources 160 (2006) 326–333.
[34] M. Ciureanu, H. Wang, J. Electrochem. Soc. 146 (1999) 4031–4040.